Periodicity of λ DNA Motions during Field Inversion Electrophoresis in Dilute Hydroxyethyl Cellulose Visualized by High-Speed Video Fluorescence Microscopy

Jeffrey J. Schwinefus and Michael D. Morris*

Department of Chemistry, University of Michigan, Ann Arbor, Michigan 48109

Received December 17, 1998; Revised Manuscript Received April 6, 1999

ABSTRACT: Using high-speed video fluorescence microscopy, we have imaged λ double-stranded (ds) DNA during both direct current (DC) and field inversion electrophoresis in dilute linear hydroxyethyl cellulose (HEC) using moderately high electric fields without the use of viscosity modifiers. The λ ds-DNA extension−contraction cycle resulting from entanglement with HEC molecules shows more periodicity with field inversion than with DC electric fields. The periodicity of the extension−contraction cycle is modulation depth- and field inversion frequency dependent. The extension−contraction kinetics of λ ds-DNA are similar in alternating and DC electric fields. We assert that modification of DNA−polymer entanglement lifetimes increases DNA motion periodicity during field inversion electrophoresis.

Introduction

Capillary electrophoresis of double-stranded (ds) DNA in dilute and semidilute linear polymers cannot resolve ds-DNA fragments larger than 40 kbp (kilobase pair) using direct current (DC) electric fields.[1−8] Above 40 kbp, ds-DNA loses size-dependent mobility in the separation medium. To extend the ds-DNA separation size range, field inversion capillary electrophoresis (FICE) was proposed in several laboratories.[1,5,8] Pulsed electric field protocols originally proved useful in extending the effective ds-DNA separation size range during gel electrophoresis.[9] Separations up to 1−2 Mbp (megabase pair) have been achieved in semidilute linear polyacrylamide[5] and dilute poly(ethylene oxide) (PEO)[2,3] using FICE. Plots of electrophoretic mobility versus DNA size showed distinct regimes with the largest changes in mobility at intermediately sized fragments.[3] Minimal change in electrophoretic mobility was observed at a given field inversion frequency or alternating current (AC) field for the smallest and largest ds-DNA fragments.

Generally, mobility dispersion is appreciable for linear ds-DNA 5 kbp and larger during DC capillary electrophoresis in linear polymers.[1,10,11] A general theory for mobility dispersion has been proposed in gels,[12,13] on the basis of classical chromatographic kinetic models.[14,15] A distribution in disentanglement times between analyte and polymer generates broad asymmetric bands. Dispersion has been shown to increase with ds-DNA size, gel or polymer concentration, and electric field strength.[10−13]

In dilute and semidilute linear polymer solutions, field inversion limits band broadening because of mobility dispersion.[1,2,10,16] FICE enhances resolution by sharpening bands without affecting ds-DNA mobilities strongly. FICE has been used to enhance DC electrophoresis resolution of φX 174 *Hae*III fragments in linear polyacrylamide[16] and ds-DNA fragments of 48.5 kbp and shorter in dilute hydroxyethyl cellulose (HEC)[2] and methyl cellulose.[1] The physics governing ds-DNA separations during field inversion are still not completely understood.

Direct visualization of individual ds-DNA molecules by fluorescence video microscopy is a powerful technique to study the electrophoretic dynamics of ds-DNA. Extensive visualization studies of DC electrophoresis in gels and polymer solutions have shown ds-DNA to cycle between random coil and extended states.[17−23] Linear ds-DNA has been observed to entangle with polymers, extending into characteristic U or J shapes followed by collapse back to the random coil. The qualitative behavior of this extension−contraction cycle is similar in gels and semidilute and dilute linear polymer solutions.

Linear ds-DNA electrophoretic dynamics are more complicated during field inversion than with DC electric fields.[23−26] The imposition of an oscillating electric field recoils the leading arms of the U- or J-shaped DNA molecules with the reverse field pulse, although this effect may have been slightly exaggerated in earlier studies.[23,24] This superimposes an extension−retraction motion upon the extended states of the ds-DNA molecule without changing the average extension of ds-DNA significantly. During field inversion, the center of mass of the ds-DNA molecule has been shown to follow the field cycle closely.[23,26]

Dilute linear polymer solutions have proven advantageous for the rapid separation of linear ds-DNA fragments in DC[27,28] and oscillating electric fields.[1,2,3] Little is known about the quantitative behavior of the linear ds-DNA extension−contraction cycle during field inversion in dilute polymer solutions. The DC electrophoretic extension−contraction periodicity of linear ds-DNA has been examined in gels using an averaged autocorrelation function.[19] The studies show some periodicity in the migration of T4 ds-DNA (166 kbp), although similar correlation analysis failed to show any significant periodicity during sinusoidal field inversion gel electrophoresis.[26] Larsson and Åkerman[20] found the distribution of T2 (167 kbp) period times to be asymmetric and wide in agarose gels with DC electric fields, although coherence of DNA molecular motions occurred with the initial field pulse. Sabanayagam and Holzwarth argued that synchronization of ds-DNA configurations and velocity changes accounted for velocity fluctuations of bands in gels with field inversion.[29] The band velocity

10.1021/ma9819384 CCC: $18.00
Published on Web 05/13/1999

fluctuations indicated that motion correlation persisted over one extension−contraction cycle. The ramifications of the synchronization of ds-DNA motions were left unresolved.

The remarkable band sharpening during dilute polymer solution FICE argues that synchronization of linear ds-DNA electrophoretic motions may occur. Periodic capture and release of polymers by ds-DNA would narrow the distribution of ds-DNA−polymer lifetimes. The result would be a narrow distribution in mobilities and diminished mobility dispersion.

In this paper, we use high-speed video (222 frames/s) fluorescence microscopy to visualize monodisperse linear λ ds-DNA (48.5 kbp) during both DC and field inversion electrophoresis in dilute HEC. We also explore the periodicity of the extension−contraction oscillations of λ ds-DNA during DC and field inversion electrophoresis.

Experimental Section

Materials and Methods. Hydroxyethyl cellulose (HEC, M_n = 438 800, Aqualon) was used as the linear polymer. The entanglement threshold for this HEC polymer has been determined by viscosity measurements to be 0.09% w/w.[27] Polymer solutions of 0.008% w/w in 1X TBE (89 mM Tris, 89 mM boric acid, 2 mM EDTA) were stirred for 24 h to ensure complete solvation of the polymer. To reduce photobleaching of the DNA sample, 2-mercaptoethanol was added (4% w/w).

Monodisperse λ ds-DNA (New England Biolabs, 48.5 kbp, contour length 16.5 μm) was diluted to 1.4 ng/μL in 1X TBE from stock solutions. The DNA samples were intercalated with POPO-3 (Molecular Probes) in 1X TBE prior to visualization. Solutions were prepared by adding 3 μL of λ ds-DNA solution to 93 μL of 0.008% HEC and 4% mercaptoethanol in 1X TBE. The final λ ds-DNA concentration of 0.04 ng/μL was sufficiently low to avoid aggregation of DNA molecules.[30] Imaging was performed in solutions with a nominal ratio of 1 dye molecule/5 base pairs.

Aliquots of sample (10 μL) were pipetted between two coverslips coated with polyacrylamide to prevent electroosmosis.[31] Two opposite sides were secured with fingernail polish to prevent leakage. The cemented coverslips containing sample were placed on a microscope glass slide fitted with platinum electrodes spaced 2.5 cm apart. The spaces between coverslips and electrodes were filled with 1% HEC solution to complete the electrical circuit.

Instrumentation. The imaging system consisted of an Olympus BH-2 infinity-corrected microscope equipped with a 50X/1.0 water immersion objective (Leitz, Rockleigh, NJ). Epi-illumination was with 60−70 mW 532 nm laser excitation through an optical fiber vibrated at 500−1000 Hz to break up laser coherence. Individual λ ds-DNA molecules were observed with an 8-bit progressive scan video camera (Pulnix, model TM-6701AN, Sunnyvale, CA) in 100-line mode (130 or 222 frames/s, 640 × 100 pixel frame) mounted on a lens-coupled intensifier (Videoscope, Sterling, VA). All data analysis used images obtained at 222 frames/s. Data collection to computer memory (DMA) was with a 60 MHz frame grabber (PDI, model IMAXX/PCI MM, Redmond, WA) installed in a Pentium-equipped computer.

A high-voltage amplifier (Trek 20/20, Medina, NY) supplied the electrophoresis voltages and was driven by a D/A board programmed with a locally written C program. The DC electric field component of 100 V/cm was the same in both DC and field inversion experiments. In field inversion experiments, 20, 35, and 50 Hz square waveforms were used. Modulation depths (V_{AC}/V_{DC}) of 110% and 180% were employed. Because of the short distance and low resistance between electrodes, waveforms were not seriously distorted by double-layer capacitance.[32]

Image Analysis. Image analysis was performed in IPLab (Signal Analytics Corp., Viennna, VA). Image processing involved median filtering, segmentation, and dilation of segments. The ds-DNA center of mass and intensity moments as defined by Oana et al.[19] were used to calculate the center of mass velocity (V_x) and extension parallel (R_l) and transverse (R_s) to the electric field. Physically, R_l and R_s are one-quarter of the major and minor axes, respectively, of an ellipse defining the DNA molecule, assuming DNA segments are uniformly distributed throughout the ellipse. V_x was calculated as a Savitsky−Golay derivative of the center of mass position of the DNA molecule using a time increment of 1 frame (4.5 ms).[33] R_l and R_s data were not smoothed. Autocorrelation[19] of λ ds-DNA V_x and R_l profiles were calculated according to eq 1,

$$Ayy(\tau) = \frac{\int [y(t+\tau) - \bar{y}][y(t) - \bar{y}]\, dt}{\int [y(t) - \bar{y}]^2\, dt} \quad (1)$$

using a locally written C program implementing a *Numerical Recipes* algorithm.[34] In eq 1 $y(t)$ is the function that is to be autocorrelated and $\bar{y}$ is the time average of $y(t)$.

The analysis of the $R_l(t)$ profile was similar to that of Oana et al.[19] To calculate the average $R_l(t)$ profile at a given field condition, approximately 15−20 peaks that were larger or equal to the time average of $R_l(t)$ plus one standard deviation in $R_l(t)$ were chosen from the plots of $R_l(t)$. The chosen maxima in $R_l(t)$ were set to a time t_m. We then took the average of the $R_l(t)$ profiles and normalized the result with the average maximum, $\bar{R}_{l\,max}$. The results were plotted versus $t - t_m$.

Results

Image Data. At 222 frames/s, it was possible to follow λ ds-DNA dynamics using analytically useful electric field and HEC concentration parameters[2,10] without the use of viscosity modifiers. Earlier electrophoresis experiments[10] established that at a DC field strength of 100 V/cm the optimum field inversion conditions in dilute HEC were 50 Hz and 180% modulation. These parameters were used in the present visualization experiments.

Figure 1 shows a time sequence (consecutive frames from a 222 frames/s series) of λ ds-DNA migrating through 0.008% HEC in an electric field of 100 V/cm. The HEC concentration is a factor of 10 below the experimentally determined entanglement threshold.[27] Upon strong entanglement with HEC, the arms of the linear DNA molecule extend forward. Eventually, one arm of the DNA forms the leading end, pulling the trailing arm off the obstacle reforming the random coil. In dilute polymer solutions, the apex of the U or J shape continues to migrate as DNA drags polymers along, unlike the situation in gels.[19,20]

The J shape in Figure 1 is representative of the majority of extended conformations of λ ds-DNA at this dilute HEC concentration. Typically, small apexes and J shapes dominate at low polymer concentrations, with few U shapes visible.[21,22]

Representative traces of the center of mass velocity and extension parallel and transverse to the electric field for λ ds-DNA in 0.008% HEC with an electric field of 100 V/cm are shown in Figure 2. The large V_x maxima result from the rapid collapse of the molecule from an extended state to the random coil because of entropic restoring forces. Maxima in V_x lag those in R_l because λ ds-DNA achieves maximum extension immediately before disengagement from entangling polymers.

The general R_l peak shape shows a slow rise to maximum extension followed by a rapid collapse back to the random coil. While collapse of a stretched polymer to the random coil is rapid, the U or J shape persists

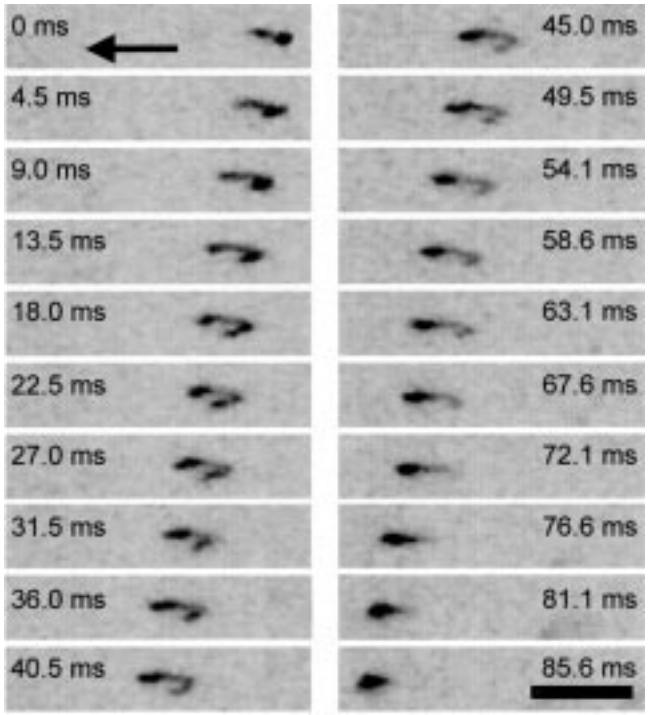

Figure 1. Time sequence of λ ds-DNA electrophoretic migration in 0.008% HEC (M_n = 438 800), 1X TBE at 100 V/cm. Consecutive frames displayed from a 222 frames/s sequence (4.5 ms between frames). Arrow indicates the direction of migration. Scale bar = 10 μm.

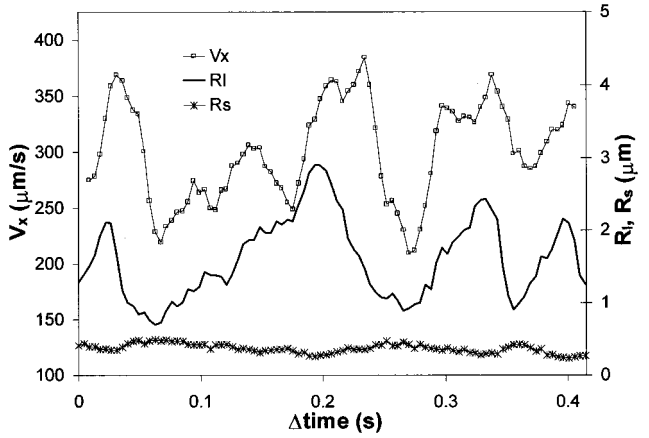

Figure 2. Representative time evolution profile of V_x, R_l, and R_s for λ ds-DNA in 0.008% HEC, 1X TBE at 100 V/cm.

because of the forces exerted on both arms. The variations in the R_l maxima reflect the variable lifetimes of the polymer−DNA aggregates.[35] The oscillations in V_x and R_l are similar to those found in gels[19] and slightly more concentrated HEC solutions.[21] R_s is constant within the limit of resolution of our experiments.

DNA secondary entanglements with HEC were observed as extended λ ds-DNA molecules contracted back to the random coil. Frequently, the collapsing end of a λ ds-DNA molecule would entangle with polymer briefly, forming a short-lived J shape with slight extension near the rear of the DNA molecule. Figure 3 shows a secondary entanglement of HEC with λ ds-DNA near the rear of the DNA molecule. As the DNA molecule collapses back to the random coil from a previous extension (0 ms), a second entanglement with HEC is observed as a slight kink along the DNA chain (7.7 ms). The DNA chain extends in a small J

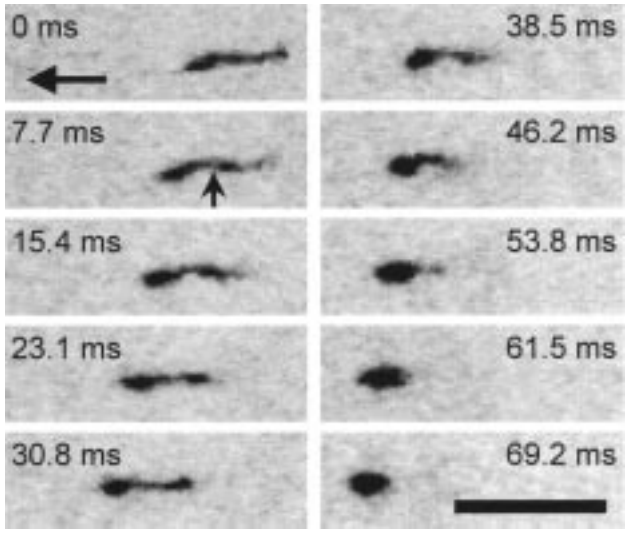

Figure 3. Secondary entanglement of λ ds-DNA with HEC near the rear of the collapsing DNA molecule. At 0 ms, the λ ds-DNA molecule is collapsing back to the random coil after a previous entanglement with HEC. The arrow pointing to the left indicates the direction of migration. The arrow pointing up indicates secondary entanglement with HEC (7.7 ms). Consecutive images are from a 130 frames/s series (7.7 ms between frames). Solution and electric field conditions are the same as in Figure 1. Scale bar = 10 μm.

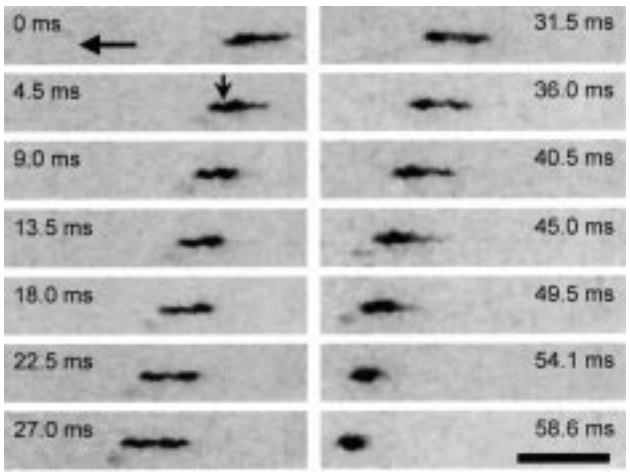

Figure 4. Secondary entanglement of λ ds-DNA with HEC within the rapidly forming random coil. At 0 ms, the λ ds-DNA is concluding a prior extension−contraction cycle, collapsing back to the random coil. The arrow pointing to the left indicates the direction of migration. The arrow pointing down indicates a secondary entanglement of HEC with this linear ds-DNA. Sequential images are from a 222 frames/s sequence (4.5 ms between frames). Solution and electric field conditions are the same as in Figure 1. Scale bar = 10 μm.

shape (15.4 and 23.1 ms) before collapsing back to the random coil.

Secondary entanglements could also occur within the rapidly forming random coil, extending the leading arm of the DNA molecule. An example of this type of secondary entanglement of λ ds-DNA with HEC is shown in Figure 4. At 0 ms, the λ ds-DNA is concluding a previous extension−contraction cycle, collapsing back into the random coil. However, collapse back to a random coil is not complete before a new cycle begins. The secondary entanglement begins at the leading portion of the DNA molecule, causing a rapid extension of a leading arm. The extension−contraction cycle is short-lived, lasting approximately 60 ms.

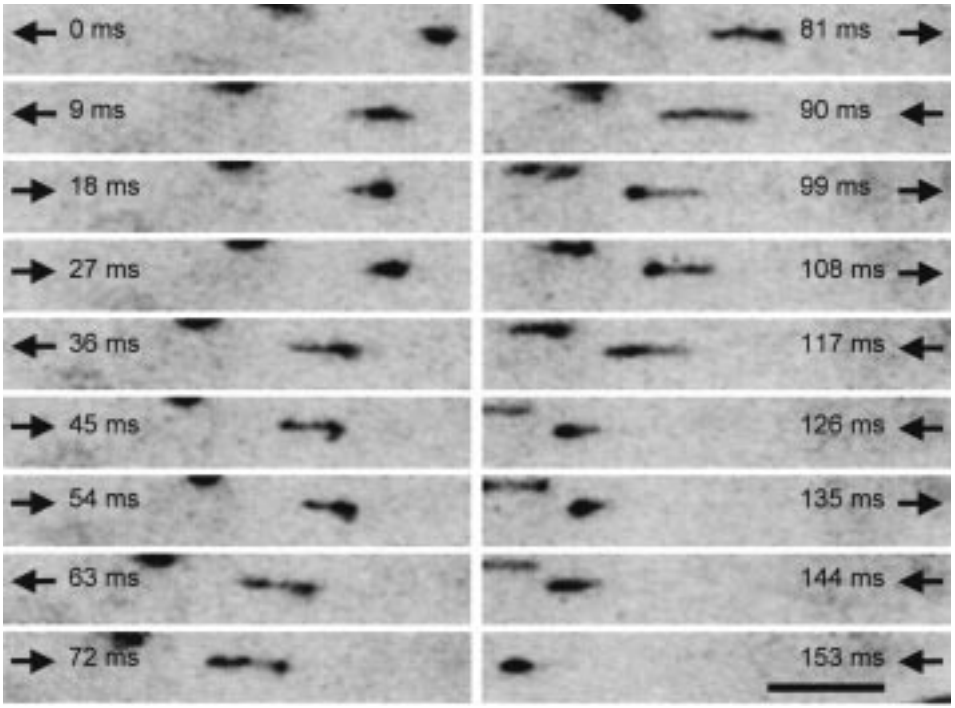

Figure 5. Field inversion time sequence of λ ds-DNA in 0.008% HEC (M_n = 438 800), 1X TBE and 100 V/cm, 180% modulation (280 V/cm forward, −80 V/cm backward), and 35 Hz square wave. Every other frame is displayed from a 222 frames/s series (9 ms between frames). Arrows indicate direction of migration. Scale bar = 10 μm.

Figure 5 contains sequential images (every other frame) of λ ds-DNA in 0.008% HEC and 100 V/cm with 180% modulation (280 V/cm forward, −80 V/cm backward) and 35 Hz square wave addition. Again, the λ ds-DNA molecule elongates into a J shape with a small apex (Figure 5, 45 and 54 ms) as in the DC regime. The extension−contraction cycle persists, but the effects of field inversion are superimposed on this motion. The molecule responds quickly to the change in electric field direction. On the negative field pulse, the apex of the J shape moves backward as the extended arms of the DNA molecule retract. The magnitude of this retraction is frequency-dependent. Several field inversion cycles pass before the molecule collapses back to the random coil.

Representative traces of V_x, R_l, and R_s for a λ ds-DNA molecule in 0.008% HEC and 100 V/cm, 180% modulation, and 50 Hz square wave are displayed in Figure 6. The center of mass velocity follows the electric field cycle closely, as in gels.[26] Similar to DC electric field behavior, maxima in V_x lag maxima in R_l. The fine oscillation structure on the R_l profile is a result of the extension and retraction of the leading arms of the DNA chain in the oscillating electric field. As in DC electric fields, R_s is fairly constant.

Time-averaged extension (n = 15−30 molecules) of λ ds-DNA in 0.008% HEC, 100 V/cm; and 180% modulation was determined to be 3.9 ± 0.6 μm at 50 Hz, 3.9 ± 0.5 μm at 35 Hz, and 3.9 ± 0.6 μm at 20 Hz. The time-averaged extension in a 100 V/cm, 110% modulation, and 50 Hz electric field was 3.7 ± 0.5 μm. These extension averages are slightly less than the DC time-averaged extension of 4.1 ± 0.5 μm.

Oscillatory Behavior. To explore the extension−contraction periodicity of λ ds-DNA during DC and pulsed electric fields, we use the autocorrelation function defined by eq 1. Figure 7 shows V_x autocorrelation functions, A_{vv}, in 0.008% HEC, 1X TBE averaged over

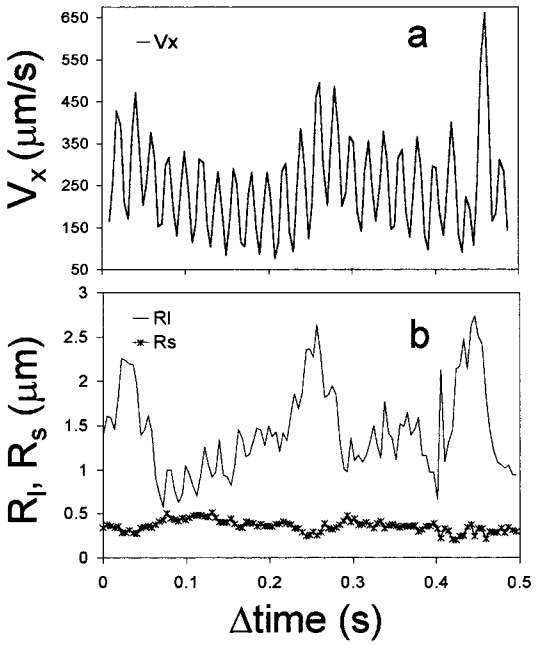

Figure 6. Representative field inversion electrophoresis time evolution profile of (a) V_x and (b) R_l and R_s for λ ds-DNA in 0.008% HEC, 1X TBE with an electric field of 100 V/cm, 180% modulation, and 50 Hz square wave.

15−30 λ ds-DNA molecules. A_{vv} at 100 V/cm (Figure 7a) does not show significant periodicity, even with extensions of 30−50% of the total contour length of λ ds-DNA. However, with field inversion, A_{vv} shows significant periodicity as expected.[26] This periodic behavior is a result of the DNA center of mass responding to the oscillating electric field rather than extension of the molecule.

We use the first maximum in the autocorrelation function to define the characteristic oscillation time τ_0. In Figure 7, field inversion characteristic oscillation

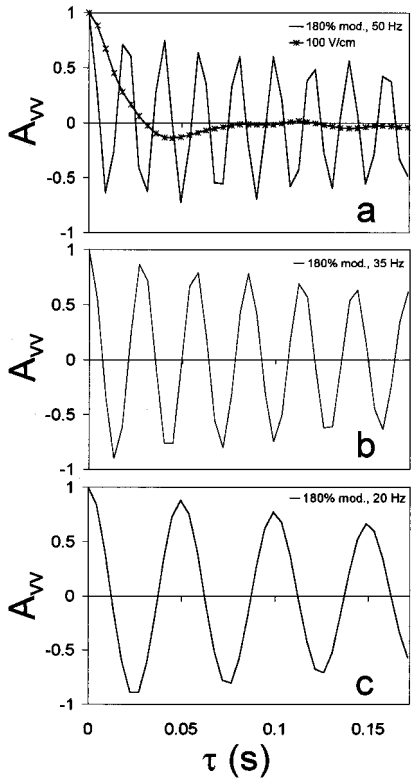

Figure 7. Average V_x autocorrelation functions, A_{vv}, for λ ds-DNA in 0.008% HEC, 1X TBE. (a)100 V/cm, 180% modulation, and 50 Hz; 100 V/cm DC. (b) 100 V/cm, 180% modulation, and 35 Hz. (c) 100 V/cm, 180% modulation, and 20 Hz. Autocorrelation functions are averaged over 15−30 molecules.

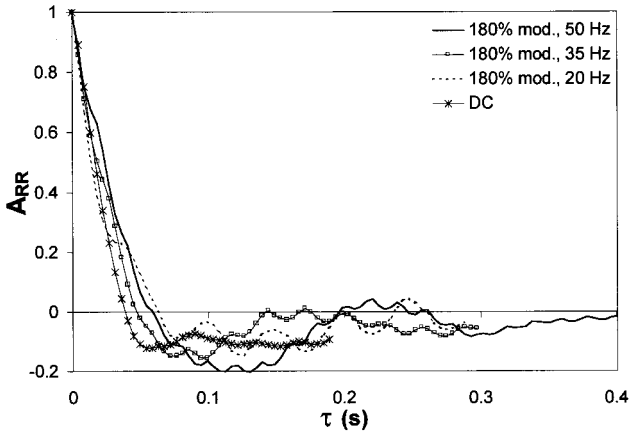

Figure 8. Average R_1 autocorrelation functions, A_{RR}, for λ ds-DNA in 0.008% HEC, 1X TBE. Electric fields of 100 V/cm DC and 100 V/cm and 180% modulation at 50, 35, and 20 Hz square wave. Autocorrelation functions are averaged over 15−30 molecules.

times are exactly the field inversion periods for all frequencies explored in this study.

The averaged R_1 autocorrelation functions, A_{RR}, for DC and field inversion are shown in Figure 8. In 0.008% HEC, 100 V/cm, A_{RR} shows little periodicity with only a slight maximum at 89 ms. Although during DC electrophoresis V_x and R_1 should oscillate with the same frequency, the average autocorrelation functions of V_x (Figure 7a) and R_1 (Figure 8) at 100 V/cm do not have the same periodicity. This behavior is a result of segment density shifting along the DNA molecule, leading to oscillations in V_x not associated with extensions in R_1.

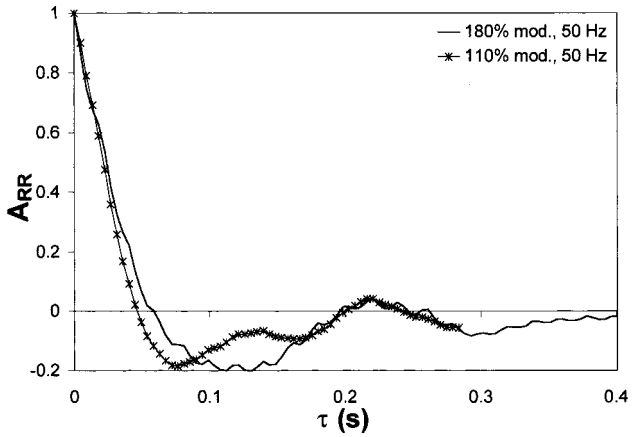

Figure 9. Dependence of R_1 autocorrelation functions of λ ds-DNA in 0.008% HEC, 1X TBE on modulation depth. Electric fields of 100 V/cm, 180% modulation and 100 V/cm, 110% modulation, and 50 Hz square wave. A_{RR} functions are averaged over 15−30 molecules.

Figure 8 shows that at 100 V/cm and 180% modulation, with increasing field inversion frequency, oscillations in R_1 become more periodic. The characteristic oscillation time maximum becomes more intense with increasing field frequency, indicating smaller variations between extension−contraction periods.

In a study of the periodicity of R_1 in gels, it was found that the characteristic oscillation time was independent of field inversion frequency for sufficiently large frequencies.[26] As seen in Figure 8, with increasing field inversion frequency, the characteristic oscillation time lengthens. Of course, the dependence of the oscillation time on field frequency would diminish at sufficiently high frequencies where DNA motions would approximate DC electric field DNA dynamics.

The characteristic oscillation times of 230 and 170 ms at 50 and 35 Hz, respectively, are greater than the corresponding field inversion periods, 20 and 28.6 ms. At 20 Hz, it is impossible to identify a characteristic oscillation time. The oscillations superimposed on A_{RR} are a result of the extension−retraction motion of DNA in an oscillating electric field. When DNA is entangled with polymer, the magnitude of the extension with the forward field pulse and retraction with the reverse field pulse are inversely proportional to field inversion frequency. In the averaged R_1 autocorrelation function, the extension−retraction oscillations in the 20 Hz oscillating electric field obscure the subsidiary maximum due to extension and collapse from the random coil.

Low modulation depths have been shown to yield poor separation resolution of large linear ds-DNA.[3] Figure 9 shows the averaged R_1 autocorrelation functions at 180% and 110% (210 V/cm forward, −10 V/cm backward) modulation, 100 V/cm, and 50 Hz square wave in 0.008% HEC, 1X TBE. At the lower modulation depth, two characteristic oscillation times become evident. The larger oscillation time coincides with the oscillation time at 180% modulation, and the smaller oscillation period is shifted closer to DC behavior. These two oscillation times indicate diminished periodicity in the electrophoretic migration of λ ds-DNA at lower field inversion modulation depths.

Extension−Contraction Profile. The mechanical nature of the DNA−polymer entanglement is a possible explanation for the increased periodicity of λ ds-DNA

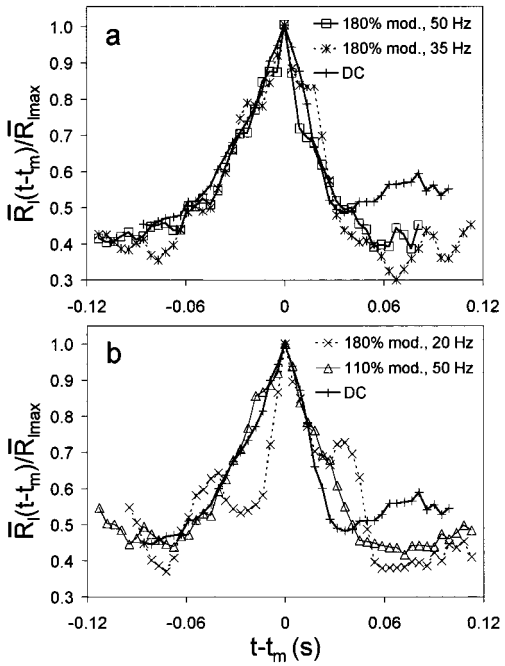

Figure 10. Average time evolution of R_l for λ ds-DNA in 0.008% HEC, 1X TBE. Profiles averaged over 10−15 individual R_l peaks at a given field condition and normalized with respect to $\bar{R}_{l\,max}$. (a) 100 V/cm DC; 100 V/cm and 180% modulation, 50 Hz, and 35 Hz. (b) 100 V/cm DC; 100 V/cm and 180% modulation, 20 Hz; 100 V/cm and 110% modulation, 50 Hz.

molecules and the decreased dispersion during field inversion capillary electrophoresis in dilute polymers.[10] To investigate the kinetics of the entanglement between λ ds-DNA and HEC, we calculated the average $R_l(t)$ profiles similar to those of the analysis of Oana et al.[19] as described in the Experimental Section. The results are shown in Figure 10.

Field inversion does not greatly affect entanglement times and collapse kinetics compared to those of DC electrophoresis. Generally, the average R_l profile shows the characteristic slow rise to the maximum before the rapid collapse back to the random coil.[19] The average R_l profiles are remarkably similar in all field conditions, except at the lowest frequency of 20 Hz. At 180% modulation and 20 Hz square wave, the extended DNA arms of the DNA/polymer aggregate retract more than at higher frequencies, generating wings on the average R_l profile.

Discussion

Figures 8 and 10 indicate a longer characteristic oscillation time with little change in the kinetics of the extension−contraction cycle with alternating electric fields. We conclude that modification of DNA−polymer interactions increases the periodicity of linear DNA motion during field inversion electrophoresis. Field inversion may eliminate weak, short-lived DNA−polymer entanglements occurring near the ends of extended DNA chains.

Starkweather and co-workers demonstrated using computer simulations that weak entanglements between DNA and polymer may occur.[36] These weak entanglements were characterized by a slight hindrance of DNA motion with little extension. In DC electric fields, we often observe secondary entanglements (Figures 3 and 4) before λ ds-DNA molecules fully collapse back to the random coil after initial entanglement with HEC. Secondary entanglements are observed only rarely at 180% modulation with a 35 or 50 Hz AC field. With reversal of the field direction, disentanglement of weakly entangled DNA−polymer aggregates may occur.

Our proposed explanation for the effect of field inversion on DNA electrophoresis in dilute polymer solutions differs from that generally accepted for electrophoresis in gels. We do not observe any significant change in average chain extension between DC and field inversion electrophoresis. Therefore, it is not surprising that the optimum inversion frequency is not close to the natural DNA inversion frequency, which is about 10 Hz in the DC field. Rather, the optimum frequency is governed by the lifetime of secondary entanglements.

The lifetime of the DNA−polymer aggregate is a function of both the lifetime of polymer with DNA and the DNA interaction lifetime with polymer.[35] Ueda and co-workers further argued that the interaction lifetime of DNA and polymer may depend on where the interaction is occurring along the DNA chain.[37] Interactions at the ends of the linear ds-DNA molecule may be fairly brief, whereas interactions at half the contour length of the DNA chain may result in long-lived U-shaped entities.

With elimination of secondary and brief entanglements by field inversion, DNA motions become more periodic. The periodicity of the extension−contraction cycle of DNA increases with field inversion, although there is little effect on the average extension−collapse dynamics of the DNA chain. With more periodic DNA electrophoretic motion, dispersion is decreased and a narrow mobility distribution results.

Capillary electrophoresis studies in conditions similar to those used here have shown λ ds-DNA bandwidths to decrease with increasing modulation depth and field frequency.[10] Larger modulation depths are necessary to drive the DNA chain sufficiently in the reverse direction, disentangling weak polymer−DNA aggregates. Low modulation depths have proven ineffective in the separation of large linear ds-DNA fragments.[3] Correlation analysis (Figure 9) at 110% modulation indicates two major oscillation period times. As in the general chromatographic case,[14,15] two modes of interaction between DNA and polymer can lead to significant band broadening.

Optimal frequencies for large linear ds-DNA separations are also chain-length-dependent.[3] A given field inversion frequency accesses a narrow range over which separations are effective. Large linear DNA fragments require lower frequencies for effective separations. Low field inversion frequencies allow more DNA reorientation during the reverse field pulse, modifying interactions with polymer along the chain.

Additional influences on DNA motion correlation are possible. Local electroosmotic flows may couple DNA motions as the field direction is reversed. Large modulation depths used in field inversion electrophoresis would contribute to this effect. Testing this contribution to DNA motion synchronization during field inversion would require varying DNA size, concentration, and ζ potential to observe breakdown of any motion correlation.

Acknowledgment. We gratefully acknowledge support from the National Institutes of Health through Grant R01-GM37006 to M.D.M. We also thank Dr. Steve

Parus for programs used to generate electrophoresis control voltages.

References and Notes

(1) Kim, Y.; Morris, M. D. *Anal. Chem.* **1994**, *66*, 3081−3085.
(2) Kim, Y.; Morris, M. D. *Anal. Chem.* **1995**, *67*, 784−786.
(3) Kim, Y.; Morris, M. D. *Electrophoresis* **1996**, *17*, 152−160.
(4) Madabhushi, R. S.; Vainer, M.; Dolnik, V.; Enad, S.; Barker, D. L.; Harris, D. W.; Mansfield, E. S. *Electrophoresis* **1997**, *18*, 104−111.
(5) Sudor, J.; Novotny, M. V. *Anal. Chem.* **1994**, *66*, 2446−2450.
(6) Sudor, J.; Novotny, M. V. *Anal. Chem.* **1994**, *66*, 2139−2147.
(7) Sudor, J.; Novotny, M. V. *Nucleic Acids Res.* **1995**, *23*, 2538−2543.
(8) Heller, C.; Pakleza, C.; Viovy, J. L. *Electrophoresis* **1995**, *16*, 1423−1428.
(9) Schwartz, D. C.; Cantor, C. R. *Cell* **1984**, *37*, 2446−2450.
(10) Schwinefus, J. J.; Morris, M. D. *Analyst* **1998**, *123*, 1481−1485.
(11) Gibson, T. J.; Sepaniak, M. J. *J. Chromatogr. B* **1997**, *695*, 103−111.
(12) Weiss, G. H.; Sokoloff, H.; Zakharov, S. F.; Chrambach, A. *Electrophoresis* **1996**, *17*, 1325−1332.
(13) Yarmola, E.; Calabrese, P. P.; Chrambach, A.; Weiss, G. H. *J. Phys. Chem. B* **1997**, *101*, 2381−2387.
(14) Giddings, J. C. *J. Chem. Phys.* **1957**, *26*, 169−173.
(15) Giddings, J. C. *Anal. Chem.* **1963**, *35*, 1999−2002.
(16) Navin, M. J.; Rapp, T. L.; Morris, M. D. *Anal. Chem.* **1994**, *66*, 1179−1182.
(17) Smith, S. B.; Aldridge, P. K.; Callis, J. B. *Science* **1989**, *243*, 203−206.
(18) Schwartz, D. C.; Koval, M. *Nature* **1989**, *338*, 520−522.
(19) Oana, H.; Masubuchi, Y.; Matsumoto, M.; Doi, M.; Matsuzawa, Y.; Yoshikawa, K. *Macromolecules* **1994**, *27*, 6061−6067.
(20) Larsson, A.; Åkerman, B. *Macromolecules* **1995**, *28*, 4441−4454.
(21) Shi, X.; Hammond, R. W.; Morris, M. D. *Anal. Chem.* **1995**, *67*, 1132−1138.
(22) Carlsson, C.; Larsson, A.; Jonsson, M.; Nordén, B. *J. Am. Chem. Soc.* **1995**, *117*, 3871−3872.
(23) Shi, X.; Hammond, R. W.; Morris, M. D. *Anal. Chem.* **1995**, *67*, 3219−3222.
(24) Hammond, R. W.; Shi, X.; Morris, M. D. *J. Microcolumn Sep.* **1996**, *8*, 201−210.
(25) Rampino, N. J.; Chrambach, A. *Biopolymers* **1991**, *31*, 1297−1307.
(26) Masubuchi, Y.; Oana, H.; Matsumoto, M.; Doi, M.; Yoshikawa, K. *Electrophoresis* **1996**, *17*, 1065−1074.
(27) Barron, A. E.; Soane, D. S.; Blanch, H. W. *J. Chromatogr.* **1993**, *652*, 3−16.
(28) Barron, A. E.; Blanch, H. W.; Soane, D. S. *Electrophoresis* **1994**, *15*, 597−615.
(29) Sabanayagam, C. R.; Holzwarth, G. *Electrophoresis* **1996**, *17*, 1052−1059.
(30) Mitnik, L.; Heller, C.; Prost, J.; Viovy, J. L. *Science* **1995**, *267*, 219−222.
(31) Hjerten, S. J. *J. Chromatogr.* **1985**, *347*, 191−198.
(32) Heiger, D. N.; Carson, S. M.; Cohen, A. S.; Karger, B. L. *Anal. Chem.* **1992**, *64*, 192−199.
(33) Savitzky, A.; Golay, M. J. E. *Anal. Chem.* **1964**, *36*, 1627−1639.
(34) Press, W. H.; Teukolsky, S. A.; Vetterling, W. T.; Flannery, B. P. *Numerical Recipes in C*, 2nd ed.; Cambridge University Press: New York, 1992; p 545.
(35) Hubert, S. J.; Slater, G. W.; Viovy, J.-L. *Macromolecules* **1996**, *29*, 1006−1009.
(36) Starkweather, M. E.; Muthukumar, M.; Hoagland, D. A. *Macromolecules* **1998**, *31*, 5495−5501.
(37) Ueda, M.; Oana, H.; Baba, Y.; Doi, M.; Yoshikawa, K. *Biophys. Chem.* **1998**, *71*, 113−123.

MA9819384